REPORT No. 893

VELOCITY DISTRIBUTIONS ON TWO-DIMENSIONAL WING-DUCT INLETS BY CONFORMAL MAPPING

By W. Perl and H. E. Moses

SUMMARY

The conformal-mapping method of the Cartesian mapping function is applied to the determination of the velocity distribution on arbitary two-dimensional duct-inlet shapes such as are used in wing installations. An idealized form of the actual wing-duct inlet is analyzed. The effects of leading-edge stagger, inlet-velocity ratio, and section lift coefficient on the velocity distribution are included in the analysis. Numerical examples are given and, in part, compared with experimental data.

INTRODUCTION

Inlet contours for wing-duct installations, such as those used to conduct cooling air to engines, are generally designed on a more empirical basis than airfoil sections because the geometry of a wing-duct inlet, and hence the determination of its velocity distribution, is more complex than that of an airfoil section. By means of the conformal-mapping method of reference 1, however, the ideal incompressible velocity distribution over two-dimensional wing-duct inlets for arbitrary lift coefficients can be calculated with about the same labor as in the corresponding calculation for an isolated airfoil.

This method was applied to an arbitrary two-dimensional wing-duct-inlet section at the NACA Cleveland laboratory in 1945 and the application is presented herein. The theory is illustrated by numerical examples, which are, in part, compared with experimental data.

ANALYSIS

SYMBOLS

The more important symbols used in the paper are listed here. All velocities are expressed as fractions of the free-stream velocity; that is, the free-stream velocity is taken as unity.

c	chord of duct-inlet section
c_l	section lift coefficient
d	horizontal distance between leading edges of duct inlet
h	vertical distance between leading edges of duct inlet
r	stagger ratio in ζ-plane
s	stagger ratio d/h in z-plane
v	velocity on surface of duct inlet
$v_{D\infty}$	velocity infinitely far inside duct
v_n	velocity at duct inlet
p	plane of circle
z	plane of duct-inlet section $(x+iy)$
ζ	plane of chord lines $(\xi+i\eta)$

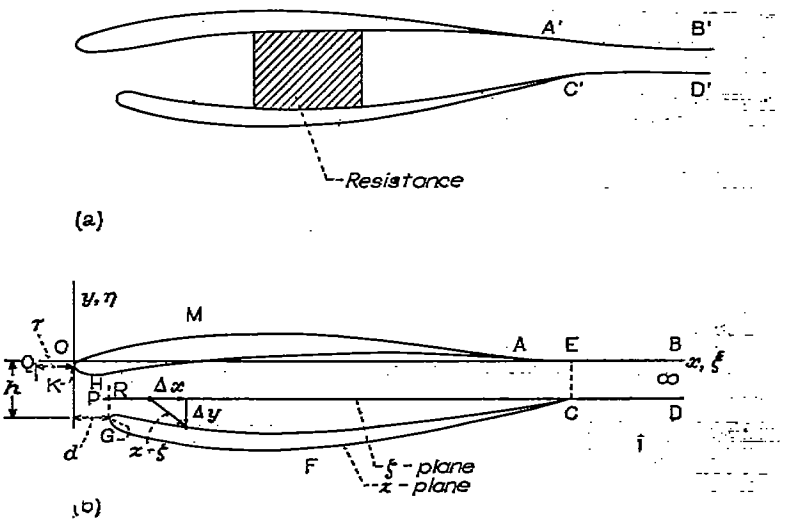

(a) Actual.
(b) Analyzed.

FIGURE 1.—Wing-duct installation.

THE CONFORMAL TRANSFORMATION

The actual two-dimensional wing-duct configuration of figure 1(a) is replaced by the contour shown in figure 1(b). The two changes made in the original configuration are (a) removal of the internal flow resistance, and (b) replacement of the streamlines A′B′ and C′D′ by the parallel, straight, rigid boundaries AB and CD. Change (a) results in a flow field of constant total pressure, and change (b) in a simply connected flow field. The analysis is thereby considerably simplified. Both effects associated with the replaced features, namely, variable inlet-velocity ratio and angle of attack, respectively, can be adequately represented in the flow function for the simplified configuration. For conventional wing-duct installations, the region of interest at the inlet, as regards velocity distribution, is sufficiently far from the region in which changes (a) and (b) were made that their influence on the required velocity distributions is negligible. (See section Illustrative Examples.)

The simplified duct-inlet contour in the z-plane is now conformally mapped onto the staggered semi-infinite parallel straight lines, QAB and PCD, in the ζ-plane (fig. 1 (b)). This mapping is accomplished by the Cartesian mapping function (CMF), defined as the vector distance $z-\zeta$ between conformally corresponding points in the z- and ζ-planes (reference 1); thus

$$\left.\begin{aligned} z-\zeta &= (x-\xi)+i(y-\eta) \\ &= \Delta x+i\Delta y \end{aligned}\right\} \tag{1}$$

The calculation of the CMF is carried out by considering it as a function of the central angle ϕ of the p-plane circle into which the ζ-plane contour can be conformally mapped by a known transformation. Inasmuch as $z-\zeta$ is regular on and outside of the z- or ζ-plane contours, by the conformal transformation from ζ to p it is also regular on and outside of the p-plane circle. The real and imaginary parts of the CMF on the circle itself are therefore related by

$$\Delta x(\phi) = -\frac{1}{2\pi}\int_0^{2\pi} \Delta y(\phi') \cot\frac{\phi'-\phi}{2}\, d\phi' \tag{2}$$

$$\Delta y(\phi) = \frac{1}{2\pi}\int_0^{2\pi} \Delta x(\phi') \cot\frac{\phi'-\phi}{2}\, d\phi' \tag{3}$$

The conformal transformation of the ζ-plane, staggered semi-infinite parallel lines, into the p-plane circle is carried out in two steps. In the first step a Schwarz-Christoffel transformation takes the ζ-plane polygon into the real axis of a t-plane such that the upper-half t-plane corresponds to the ζ-plane. With the correspondence of boundary points indicated in figure 2, this transformation is (reference 2):

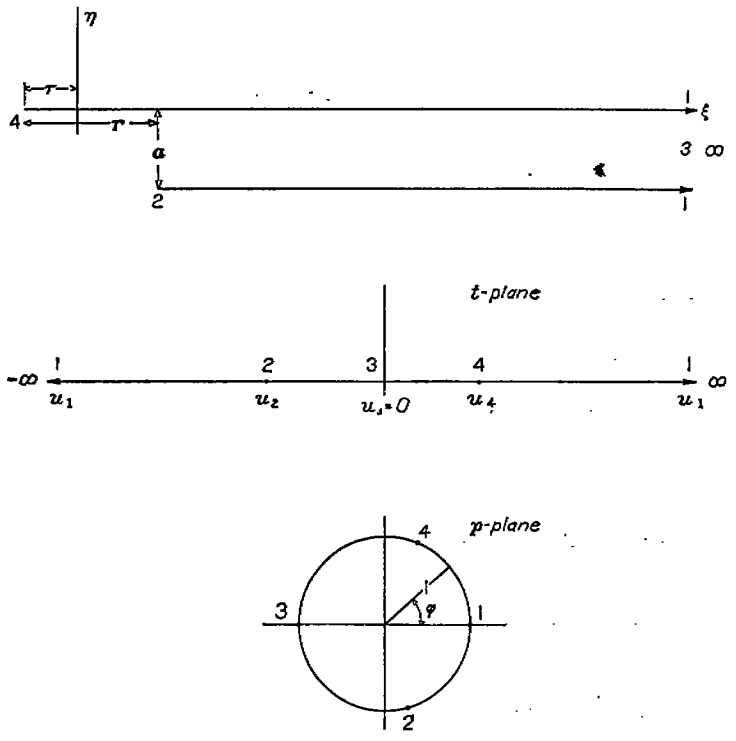

FIGURE 2.—Conformal relation of ζ-, t-, and p-planes.

$$\frac{d\zeta}{dt} = C_1\frac{(t-u_2)(t-u_4)}{t} \tag{4}$$

$$\zeta = C_1\left[\frac{t^2}{2}-(u_2+u_4)t+u_2u_4\log_e t\right]+C_2 \tag{5}$$

The six constants given by u_2, u_4 (real), and C_1, C_2 (complex) are determined for the orientation and the scale indicated in figure 2 by the six conditions:

(a) C_1 real (staggered lines horizontal)
(b) $a=1$, scale factor in ζ-plane
(c) r equals desired stagger in ζ-plane, $\zeta(u_2)=r+\tau-i$
(d) $u_2=-1$, scale factor in t-plane
(e) upper leading edge in ζ-plane at point $(\tau, 0)$ or $\zeta(u_4)=\tau$ (two conditions)

The constant τ is inserted in condition (e) in order to locate the leading edge of the upper inlet section tangent to the y-axis. By use of the foregoing conditions, equation (5) reduces to

$$\zeta = \frac{1}{\pi}\left(\frac{t}{m}-1\right)\left[\frac{m}{2}\left(\frac{t}{m}-1\right)+1\right]-\frac{1}{\pi}\log_e\frac{t}{m}+\tau \tag{6}$$

The quantity $m\equiv u_4$ is the following function of the stagger ratio r:

$$\pi r = \log_e m+\frac{1}{2}\left(m-\frac{1}{m}\right) \tag{7}$$

Equation (7) is plotted in figure 3.

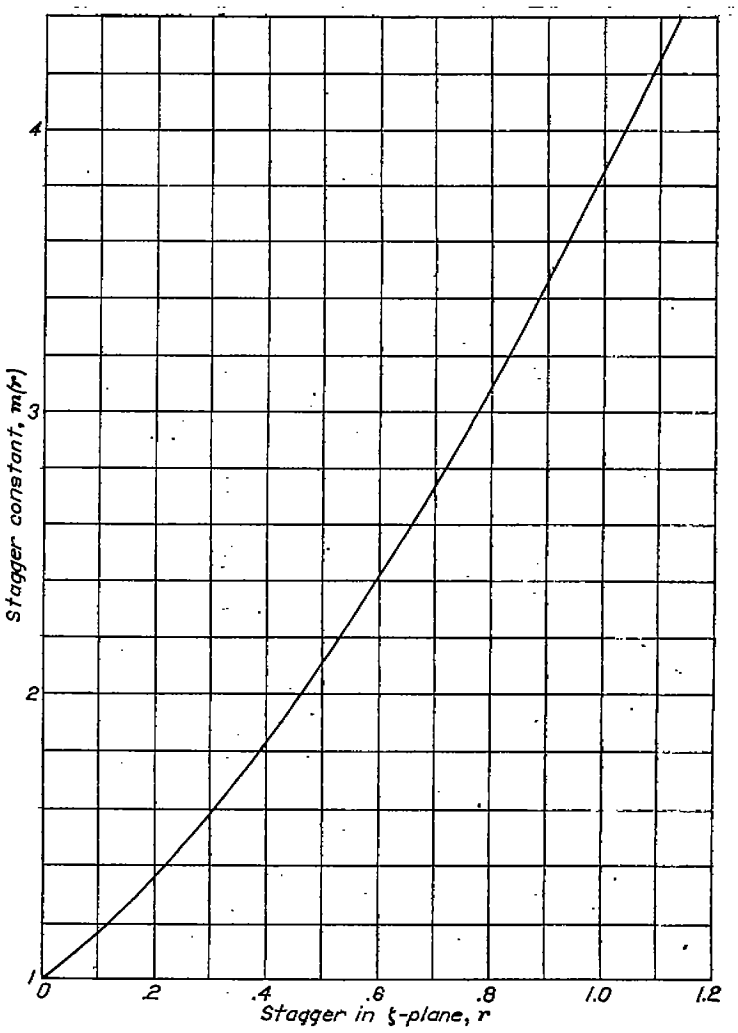

FIGURE 3.—Stagger constant as a function of stagger in ζ-plane.

The second step of the desired transformation from ζ to p consists in mapping the upper-half t-plane onto the region outside of the p-plane unit circle by a bilinear transformation, here taken as

$$t=i\left(\frac{p+1}{p-1}\right) \tag{8}$$

The correspondence of points for equation (8) is indicated in figure 2. The use of other bilinear transformations is discussed in the section Illustrative Examples.

Equations (1), (6), and (8) constitute the conformal transformation from the region around the duct-inlet section in the physical z-plane to the region outside the unit circle p-plane. These equations, with $p=e^{i\phi}$, give for conformally corresponding points on the boundaries

$$t=\cot\frac{\phi}{2} \tag{9}$$

$$\left.\begin{aligned} x&=\xi+\Delta x \\ x&=\frac{1}{\pi}\left(\frac{1}{m}\cot\frac{\phi}{2}-1\right)\left[\frac{m}{2}\left(\frac{1}{m}\cot\frac{\phi}{2}-1\right)+1\right]- \\ &\quad\frac{1}{\pi}\log_e\frac{1}{m}\left|\cot\frac{\phi}{2}\right|+\Delta x(\phi)+\tau \end{aligned}\right\} \tag{10}$$

$$\left.\begin{aligned} y&=\eta+\Delta y \\ y&=\Delta y(\phi) \qquad 0<\phi<\pi \text{ upper-duct inlet section} \\ y&=\Delta y(\phi)-1 \qquad \pi<\phi<2\pi \text{ lower-duct inlet section} \end{aligned}\right\} \tag{11}$$

The leading-edge points of the upper-duct- and lower-duct-inlet sections may be defined as the upstream points of tangency of normals from the "chord" lines OA and RC with the duct-inlet contours (fig. 1 (b)). These points may be found as functions of ϕ by minimizing x with respect to ϕ in equation (10). The resulting condition is

$$\frac{d\Delta x}{d\phi}=\frac{\left(\cot\frac{\phi}{2}-m\right)\left(\cot\frac{\phi}{2}+1\right)}{\pi m\sin\phi} \tag{12}$$

VELOCITY DISTRIBUTION

The velocity distribution on the duct-inlet section is given by

$$v=\left|\frac{dW}{dz}\right| \tag{13}$$

in which the complex potential W is

$$W=\zeta+\frac{A}{\pi}t+\frac{B}{\pi}\log_e t \tag{14}$$

The term ζ represents a uniform flow velocity to the right, of unit magnitude in the ζ-plane, and gives a free-stream velocity of unity in the physical plane. The term $\frac{A}{\pi}t$ represents a uniform flow in the t-plane and corresponds to a circulatory flow around the duct inlet in the physical plane. This term gives the effect of angle of attack on the physical duct-inlet section, although the geometric angle of attack of the section analyzed must remain zero because of its semi-infinite extent. The term $\frac{B}{\pi}\log_e t$ represents the flow due to a source at the origin in the t-plane and gives the desired inlet velocity into the duct in the physical plane.

The quantitative effect of the parameters A and B in the physical plane is determined by evaluation of the complex velocity

$$\frac{dW}{dz}=\left(1+\frac{A}{\pi}\frac{dt}{d\zeta}+\frac{B}{\pi t}\frac{dt}{d\zeta}\right)\frac{d\zeta}{dz} \tag{15}$$

where, by equation (6),

$$\frac{dt}{d\zeta}=\frac{\pi m t}{(t-m)(t+1)} \tag{16}$$

and, because $z-\zeta$ is regular on and outside of the p-plane circle,

$$z-\zeta=\sum_0^\infty\frac{c_n}{p^n} \tag{17}$$

$$\left.\begin{aligned} \frac{dz}{d\zeta}&=1-\frac{dp}{d\zeta}\sum_0^\infty\frac{nc_n}{p^{n+1}} \\ \frac{dz}{d\zeta}&=1+\frac{2i}{(t-i)^2}\frac{\pi m t}{(t-m)(t+1)}\sum_0^\infty\frac{nc_n}{p^{n+1}} \end{aligned}\right\} \tag{18}$$

Infinitely far inside the duct in the physical plane, the correspondence of points is: $z=\infty$, $\zeta=\infty$ by equation (17), $t=0$ by equation (6), and $p=-1$ by equation (8). Hence, at this point, $\frac{dz}{d\zeta}=1$ by equation (18), $\frac{dt}{d\zeta}=0$, and $\frac{1}{t}\frac{dt}{d\zeta}=-\pi$ by equation (16); and equation (15) gives for the velocity $v_{D\infty}$ infinitely far inside the duct

$$v_{D\infty}=1-B \tag{19}$$

The velocity distribution on the inner wall of the duct-inlet section becomes almost constant a short distance behind the leading edge. (See section Illustrative Examples.) The inlet velocity v_n is defined as this asymptotic value. The inlet velocity v_n will be different from $v_{D\infty}$ if the height at the inlet is different from the height (unity) infinitely far inside the duct. Infinitely far upstream of the duct-inlet section the correspondence of points is: $z=-\infty$, $\zeta=-\infty$, $t=i\infty$, and $p=1$, and consequently $\frac{dz}{d\zeta}=1$, $\frac{dt}{d\zeta}=\frac{1}{t}\frac{dt}{d\zeta}=0$. This result holds infinitely far outside the duct in any direction. Hence, the free-stream velocity is by equation (15), unity.

The quantity A may be evaluated either as a function of the stagnation-point locations on the duct inlet or as a function of a suitably defined lift coefficient. In terms of the stagnation points, given by $\frac{dW}{dz}=0$ in equation (15), and with equations (16) and (9),

$$A=\frac{(m-1)\cot\frac{\phi_{st}}{2}-\cot^2\frac{\phi_{st}}{2}+m(1-B)}{m\cot\frac{\phi_{st}}{2}} \tag{20}$$

$$\cot\frac{\phi_{st}}{2}=\frac{-[1+m(A-1)]\pm\sqrt{[1+m(A-1)]^2+4m(1-B)}}{2} \tag{21}$$

For a given A (and B) equation (21) is a quadratic equation for the two stagnation-point locations. When quantity A is alternatively regarded as a function of lift coefficient c_l, the section lift coefficient is defined in terms of circulation and chord by the well-known isolated-airfoil relation

$$c_l=\frac{2\Gamma}{c} \tag{22}$$

The chord c is defined as the over-all length of the wing-duct-inlet section in the free-stream direction (OE in fig. 1(b)), and the circulation Γ, as the line integral of the velocity over the circuit CFGHKMAEC around the wing-duct installation. This circulation can be evaluated as the sum of the potential difference over the lower surface $\Phi_G-\Phi_C$, and the potential difference over the upper surface $\Phi_E-\Phi_H$. The difference of potential over the paths GH and EC is neglected because the velocity is here approximately perpendicular to the path. Hence, by equation (14)

$$\Phi_E-\Phi_H=\xi_E-\xi_H+\frac{A}{\pi}(t_E-t_H)+\frac{B}{\pi}\log_e\frac{t_E}{t_H}$$

$$\Phi_G-\Phi_C=\xi_G-\xi_C+\frac{A}{\pi}(t_G-t_C)+\frac{B}{\pi}\log_e\frac{t_G}{t_C}$$

and

$$\left.\begin{aligned}&\Gamma=(\Phi_E-\Phi_H)+(\Phi_G-\Phi_C)\\&\Gamma=(\xi_E-\xi_C)-(\xi_H-\xi_G)+\frac{A}{\pi}[(t_E-t_C)-(t_H-t_G)]+\\&\quad\frac{B}{\pi}\log_e\left(\frac{t_Et_G}{t_Ht_C}\right)\end{aligned}\right\} \tag{23}$$

Finally, when equation (23) is solved for A, and Γ is expressed in terms of c_l by equation (22) with $c=x_E$,

$$A=\frac{\pi\left[\frac{c_l}{2}x_E-(\xi_E-\xi_C)+(\xi_H-\xi_G)\right]-B\log_e\left(\frac{t_Et_G}{t_Ht_C}\right)}{(t_E-t_C)-(t_H-t_G)} \tag{24}$$

The quantities x, ξ, and t at the various points indicated in equation (24) are given in terms of the corresponding central angle ϕ by equations (9) and (10). The various ϕ values are known when the conformal transformation of the duct inlet has been carried out.

For a CMF $\Delta x(\phi)$, $\Delta y(\phi)$, stagger constant m, and the constants A and B corresponding to the lift coefficient and the inlet-velocity ratio, the velocity distribution on the duct-inlet contour is given by the absolute magnitude of dW/dz on the boundary. On the boundary, $p=e^{i\phi}$,

$$\left.\begin{aligned}&\frac{dz}{d\xi}=1+\frac{d(z-\xi)}{d\xi}\\&\frac{dz}{d\xi}=1+\frac{d(\Delta x+i\Delta y)}{d\phi}\frac{d\phi}{dt}\frac{dt}{d\xi}\end{aligned}\right\} \tag{25}$$

Substitution of equations (9), (16), and (25) in equation (15) yields for the velocity distribution on the duct-inlet section

$$v=\frac{\left(\cot\frac{\phi}{2}-m\right)\left(\cot\frac{\phi}{2}+1\right)+mA\cot\frac{\phi}{2}+mB}{\pi m\sin\phi\sqrt{\left[\frac{\left(\cot\frac{\phi}{2}-m\right)\left(\cot\frac{\phi}{2}+1\right)}{\pi m\sin\phi}-\frac{d\Delta x}{d\phi}\right]^2+\left(\frac{d\Delta y}{d\phi}\right)^2}} \tag{26}$$

PROCEDURE FOR CALCULATION OF CMF

The calculation of the CMF $\Delta x(\phi)$, $\Delta y(\phi)$, and stagger constant m for a given duct-inlet section may be carried out by a process of successive approximations similar to that of reference 1. The steps are outlined as follows:

1. The duct-inlet section is drawn in normal form (fig. 1 (b)). Point O is the origin and the scale is such that the normal distance between the chord lines OA and RC is unity. The stagger $s=d/h$ of the duct inlet is, in general, different from the stagger r of the chord lines.

2. A set of abscissas $x(\phi)$ is calculated for a standard set of values of ϕ by equation (10). The $\Delta x(\phi)$ and τ may be that of a previous example or, at worst, equal to zero. The value of m may be taken from figure 3 for $r=s$.

3. The ordinates y of the duct-inlet contour corresponding to the abscissas x of step 2 are measured. The function $\Delta y(\phi)$ is thereby determined (equation (11)).

4. The function $\Delta x(\phi)$ is calculated from $\Delta y(\phi)$ by equation (2).

5. The functions $\Delta x(\phi)$ of step 4, $\Delta y(\phi)$ of step 3, and m of step 2 constitute by equations (10) and (11) a duct-inlet section of which the difference in abscissas between the leading edges is, in general, other than that specified. The constant m is therefore adjusted to make this difference equal to the specified value. To this end equation (12) (corresponding to the values ϕ_1 and ϕ_2 for the two extremities) and the equation for the difference d in the leading-edge abscissas

$$x(m,\phi_1)-x(m,\phi_2)=d \tag{27}$$

obtained from equation (10), can be solved simultaneously for ϕ_1, ϕ_2, and m. A more convenient procedure is one of iteration. Initial values ϕ_1 and ϕ_2 for minimum x are graphically obtained by plotting equation (10) in the necessary regions. A value of m is then obtained from equation (27). With this value of m, values of ϕ_1 and ϕ_2 are again graphically found for minimum x by equation (10). The process is continued until ϕ_1, ϕ_2, and m do not change appreciably in successive calculations. Finally, a constant τ is so chosen that $x(\phi_1)=0$. The derived inlet section is now in normal form.

6. The values of m and τ derived in step 5 and $\Delta x(\phi)$ and $\Delta y(\phi)$ of steps 4 and 3 yield a shape by equations (10) and (11), which can be compared with the given one. If the agreement is not sufficiently close, steps 3 to 5 are repeated.

7. The velocity distribution is obtained by substitution of the final m and the derivatives $\frac{d\Delta x}{d\phi}$ and $\frac{d\Delta y}{d\phi}$ of the final CMF in equation (26). The value of B is chosen to produce the desired inlet velocity (the velocity given by equation (26) on the inside walls of the duct-inlet section). The value of A is chosen to locate the stagnation points in the desired manner (equation (21)) or for a desired nominal lift coefficient (equation (24)).

The inverse problem, namely, the calculation of the duct-inlet section to produce a prescribed velocity distribution, may be treated by the methods given in references 1 and 3.

ILLUSTRATIVE EXAMPLES

As a first application of the theory, the symmetrical wing-duct installation ($m=1.0$), on which pressure distributions were measured in reference 4 (shape 9), was analyzed. The installation is shown in figure 4 and the ordinates are listed in table I. The trailing-edge portions were actually flaps

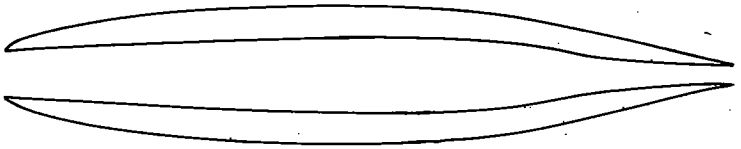

FIGURE 4.—Symmetrical duct-inlet section (reference 4, shape 9). $m=1.0$.

by which the inlet velocity was varied. The scale used for the calculation was such that the distance between trailing edges was unity, as assumed in the theory. An evenly spaced set of 48 ϕ-values was taken of which only 24 were actually used because of the symmetry. Of these 24 values, 21 were included in the front 8 percent of the chord. This portion of the duct inlet was therefore the portion effectively analyzed. The leading-edge portion is plotted in figure 5 to a scale such that the vertical distance between the leading edges, the entrance height h, is unity.

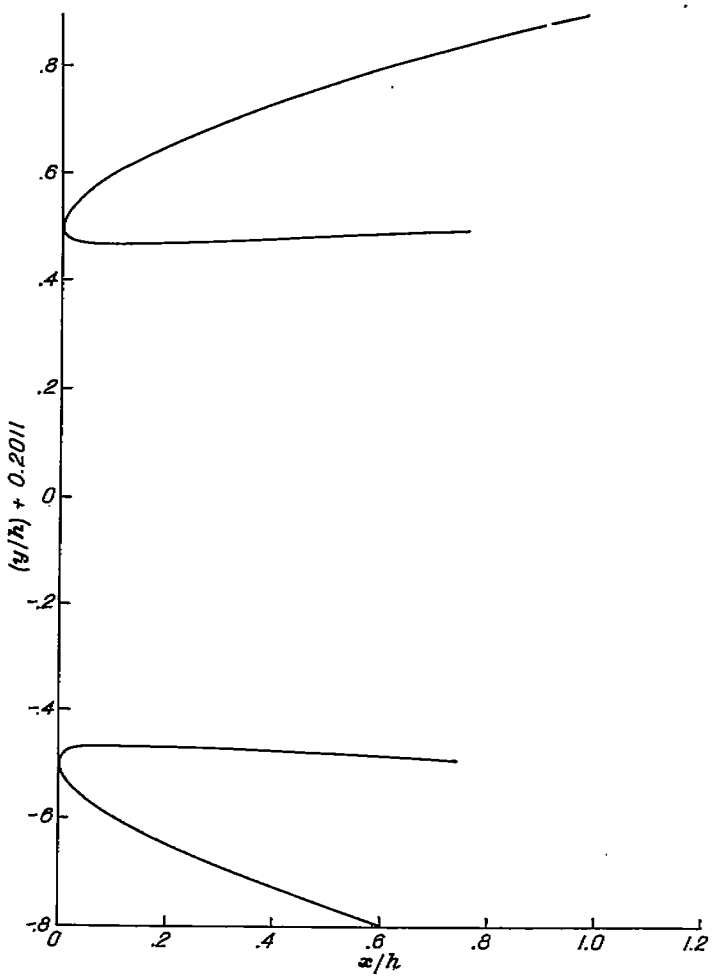

Figure 5.—Leading edge of symmetrical duct-inlet section with $s=0$ and $m=1.0$.

The CMF obtained after four approximations (which produced coincidence of the specified shape and the derived shape) is listed in table II and plotted in figure 6. In the

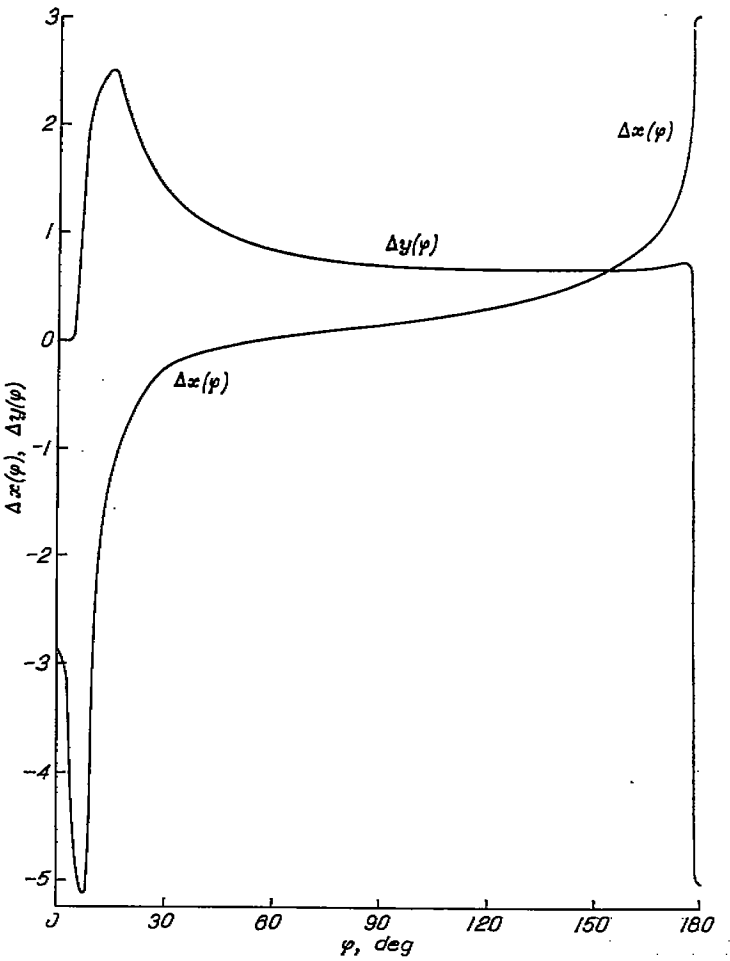

Figure 6.—Cartesian mapping function for duct-inlet sections.

first two approximations, the airfoil was drawn to an abscissa scale of 25 inches for the chord and had an ordinate scale four times the abscissa scale. The last two approximations were made for the airfoil drawn to a scale such that the chord length was 100 inches; the ordinate scale was the same as the abscissa scale. The values of Δx were computed, for the most part, by the method of numerical evaluation of conjugate functions developed in appendix C of reference 5. Near 0° and 180°, because of the rapid variation of $\Delta y(\phi)$ in these regions (fig. 6), Δx was obtained by plotting the integrand of equation (2) and graphical integration. The values of the CMF graphically obtained are indicated in table II. The velocity distributions, also listed in table II, were calculated for inlet-velocity ratios v_n of 0, 0.5, and 1.0 and for nominal lift coefficients of 0, 0.3, 0.6, 0.9, and are shown in figure 7. The derivatives of the CMF used in calculating the velocity distribution were obtained by graphical measurement from the CMF.

The velocity distribution for $c_l=0$ and $v_n=0.5$ satisfactorily checked that experimentally obtained in reference 4 for $c_l=0$ and $v_n=0.473$ (fig. 7(c)). The reason for the discrepancy between theoretical and experimental inlet-velocity ratios at which the velocity distributions agreed is not clear. Possible reasons are the changes in downstream shape required by the analysis and a difference in the method of specification of inlet-velocity ratio. The theoretical inlet velocity v_n has been defined as the constant value approached

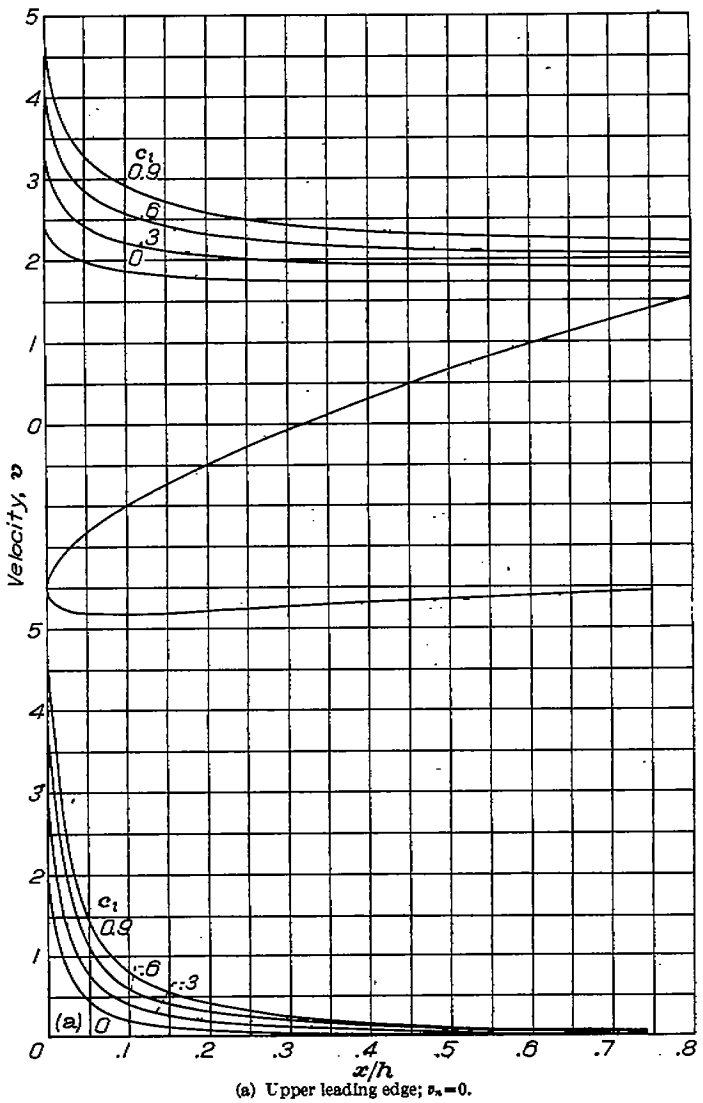

(a) Upper leading edge; $v_n=0$.

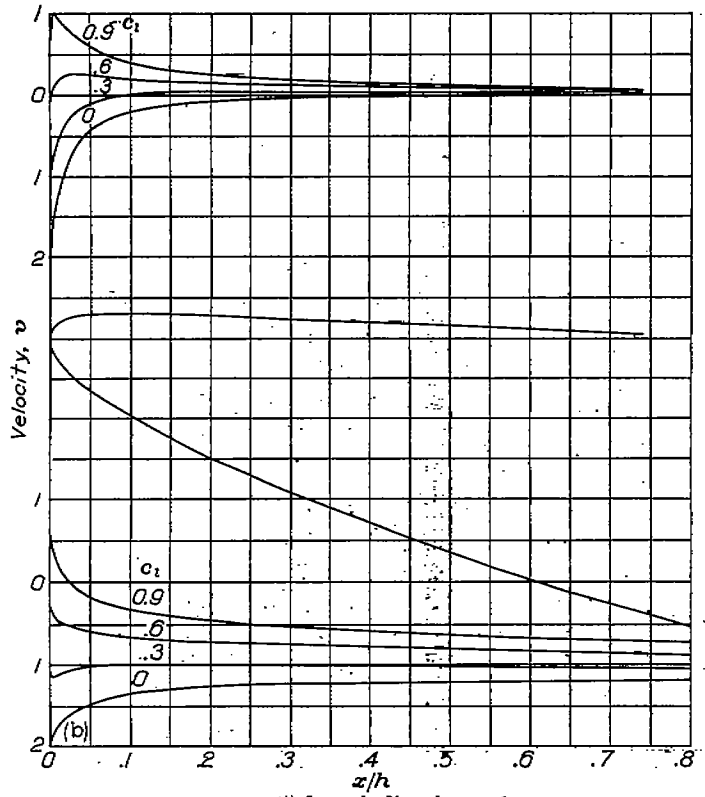

(b) Lower leading edge; $v_n=0$.

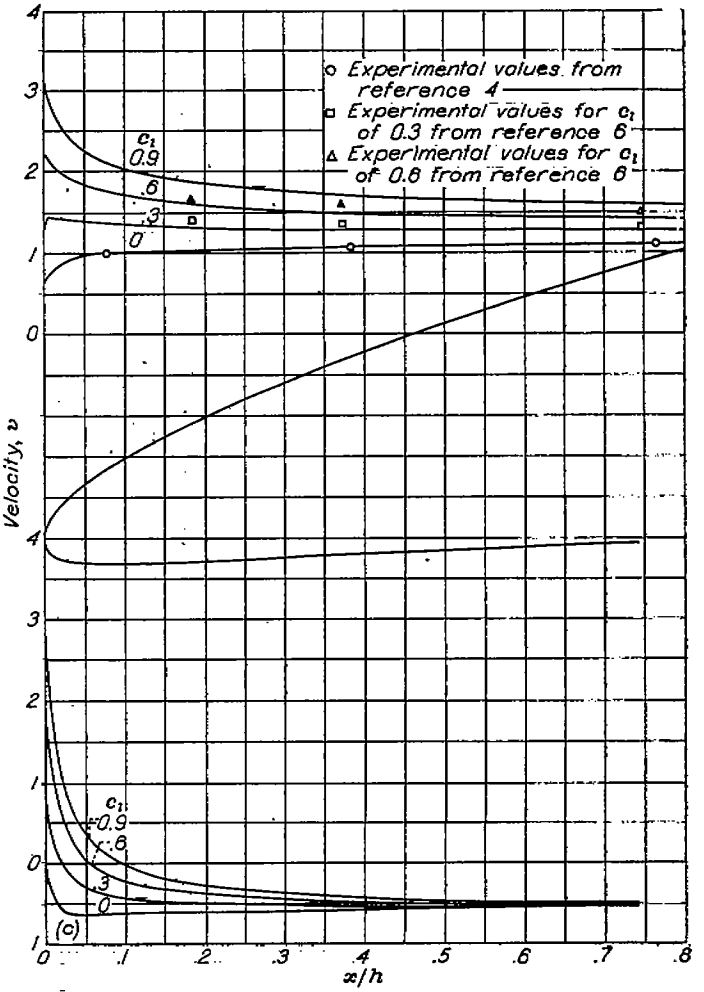

(c) Upper leading edge; $v_n=0.5$.

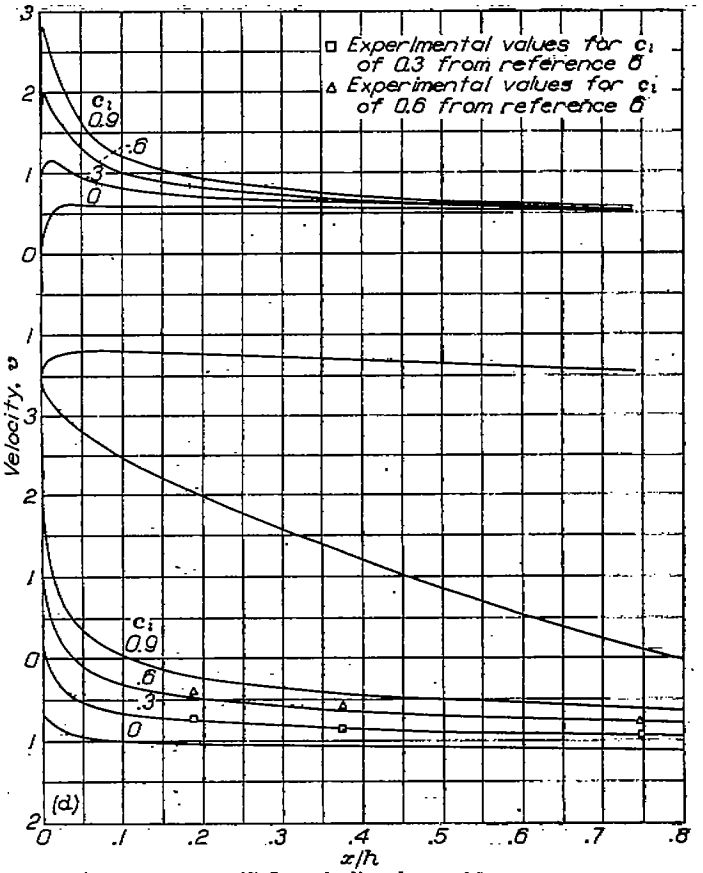

(d) Lower leading edge; $v_n=0.5$.

Figure 7.—Velocity distribution on upper and lower leading edges of symmetrical duct-inlet section with $s=0$ and $m=1.0$.

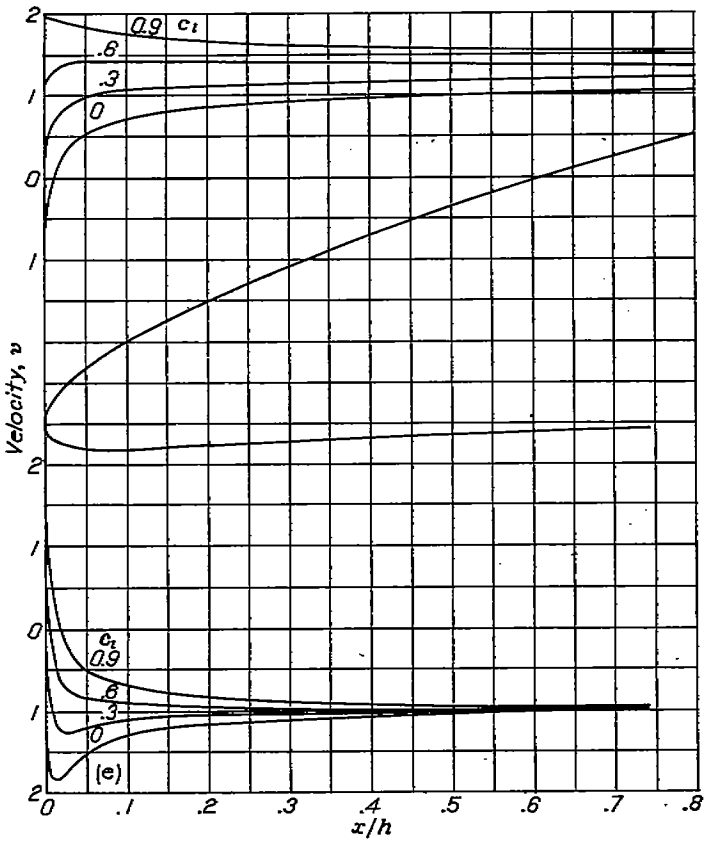

(e) Upper leading edge; $v_\infty = 1.0$.

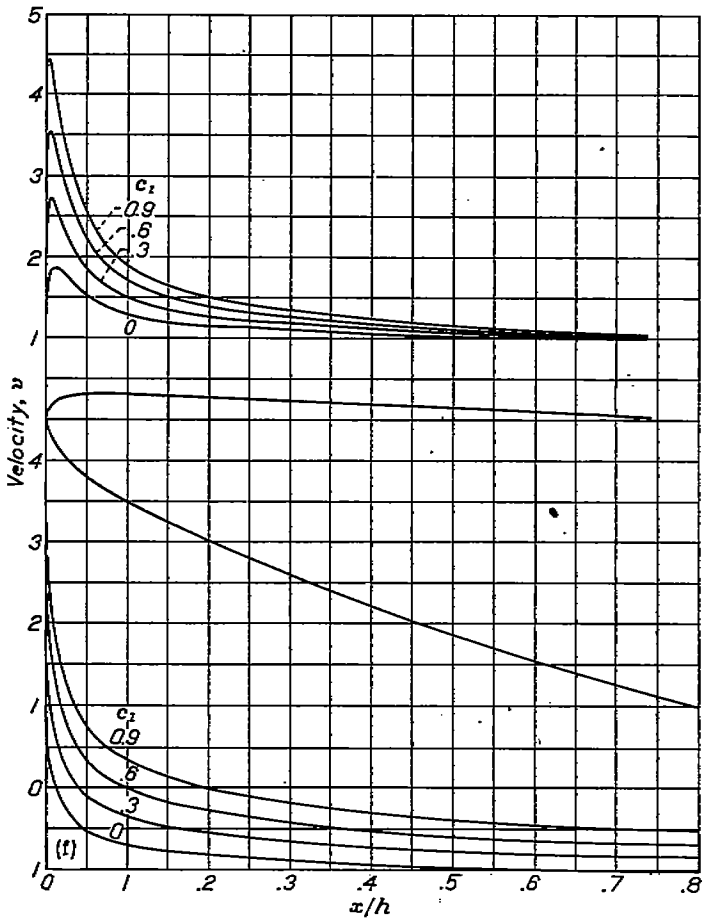

(f) Lower leading edge; $v_\infty = 1.0$.

Figure 7.—Concluded.

by the velocity on the wall of the duct at a short distance behind the leading edge. The experimental determination of the inlet-velocity ratio in reference 4 was not made entirely clear.

The velocity distributions for the c_l values 0.3 and 0.6 were also compared with the experimental data of reference 6 obtained for the same duct-inlet section at various angles of attack at a Mach number of 0.20. The comparison (given in figs. 7 (c) and 7 (d)), indicates the validity of the theoretical analysis, particularly of the derivation of the nominal section lift coefficient c_l.

The feature of the velocity distribution shown in figure 7 that should be particularly noted is the closeness to the leading edge (well within the 8-percent of the chord length that was studied) at which the greatest changes in velocity distribution occur as a result of a change in operating conditions v_∞ or c_l. This fact justifies and requires the analysis of a region very close to the inlet, that is, the concentration of the chosen set of ϕ-points close to the inlet.

In order to illustrate the use of the theory for the staggered case, $m \neq 1.0$, the CMF $\Delta x(\phi)$ and $\Delta y(\phi)$ for the symmetrical inlet was used with the m-values 1.5 and 2.0. These shapes and velocities are shown in figures 8 to 11 and are given in tables III and IV, respectively. In the graphs of the duct inlets, the ordinates have been so adjusted that the upper and lower leading edges are at 0.5 and -0.5, respectively. Although the derived shapes are different from the original

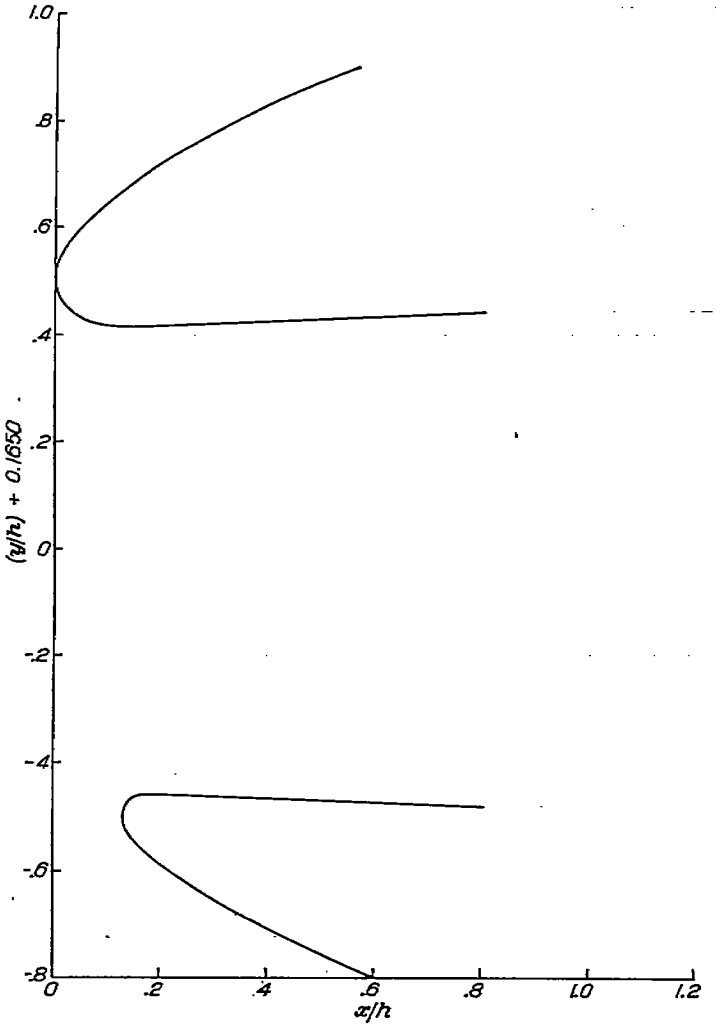

Figure 8.—Leading edge of nonsymmetrical duct-inlet section with $s = 0.132$ and $m = 1.5$.

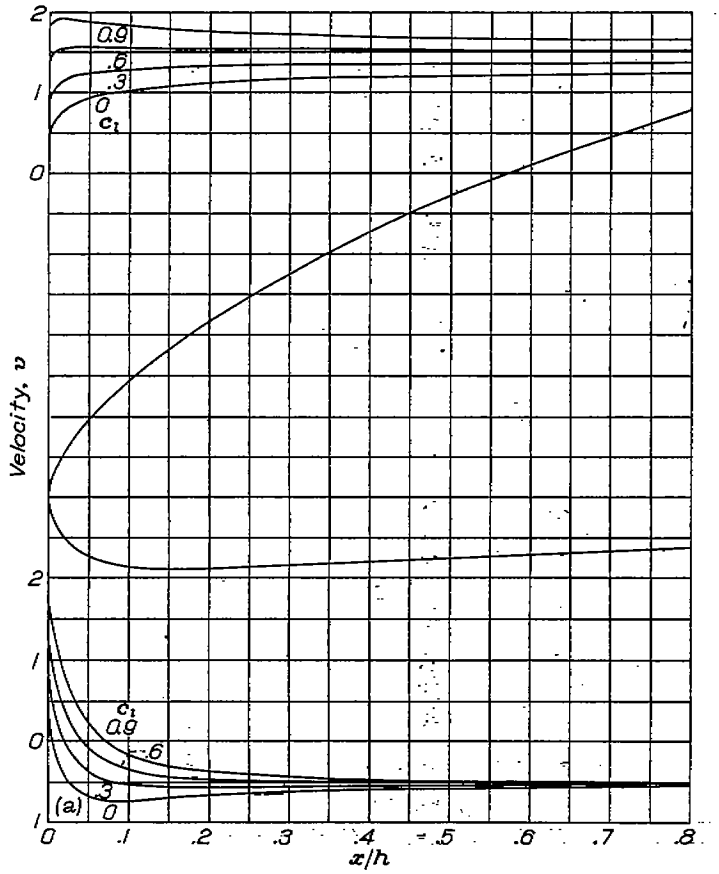

(a) Upper leading edge.

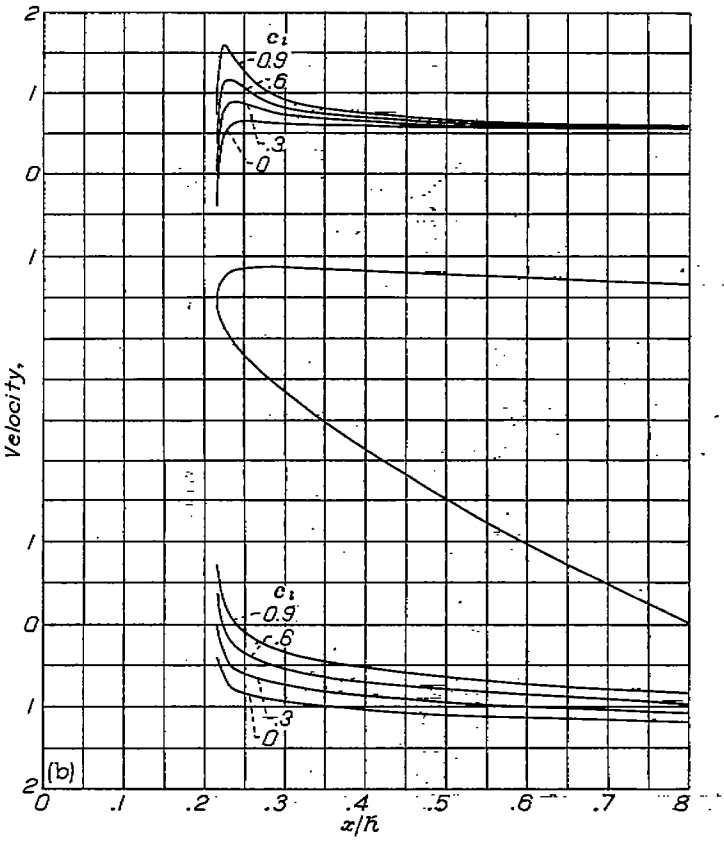

(b) Lower leading edge.

FIGURE 9.—Velocity distribution on upper and lower leading edges of nonsymmetrical duct-inlet section with $s=0.132$ and $m=1.5$. $v_n=0.5$.

unstaggered one, evidently the effect of stagger is to reduce the velocity peaks for positive lift coefficients.

When a more highly staggered inlet was derived for $m=3.0$ by the foregoing method, the upper contour of the resulting inlet was found to be excessively thick. The points in the physical plane corresponding to $\Delta x(\phi)$, $\Delta y(\phi)$, and $m=3.0$ were therefore rearranged by using the same Δx and Δy, regarded, however, as functions of θ, with θ related to ϕ by the bilinear transformation (see appendix B of reference 5)

$$p=\frac{p'+\frac{n-1}{n+1}}{\frac{n-1}{n+1}p'+1} \tag{28}$$

in which, on the p- and p'-plane unit circles corresponding to the duct-inlet contour,

$$p=e^{i\phi}, p'=e^{i\theta} \tag{29}$$

The choice $n=1.5$ produced the shape shown in figure 12. The ordinates are listed in table V. It should be noted that the use of an auxiliary bilinear transformation (equation (28), for example) provides a very flexible and convenient method of distributing a given number of mapping points in the optimum manner. The auxiliary bilinear transformation may also be used to smooth out a sharply peaked function of ϕ to make its conjugate more easily calculable.

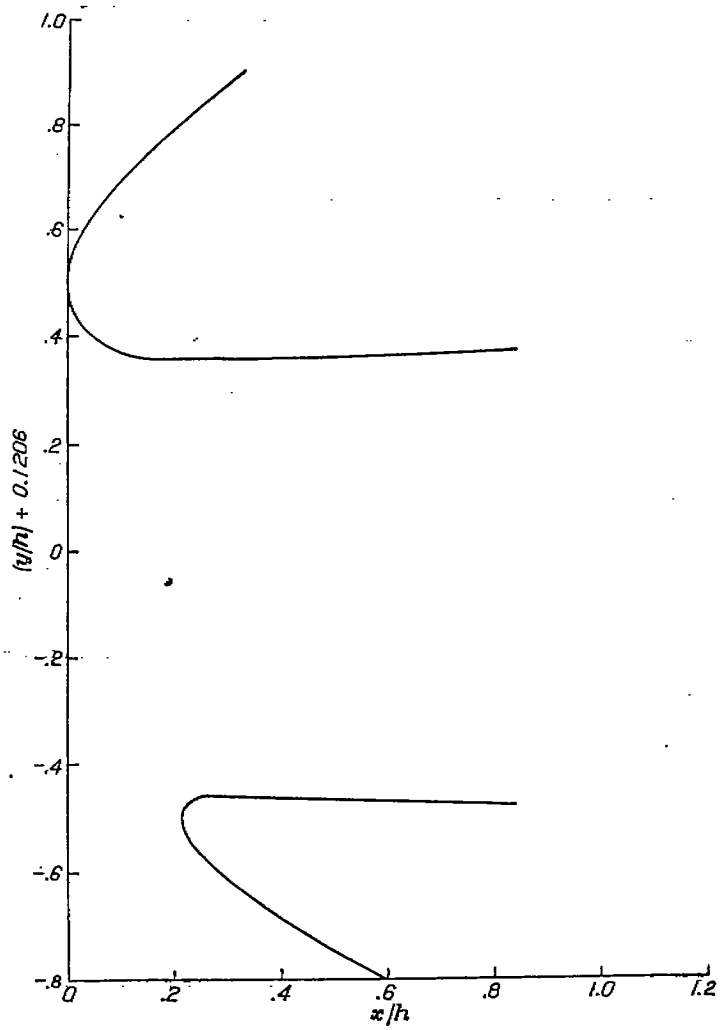

FIGURE 10.—Leading edge of nonsymmetrical duct-inlet section with $s=0.215$ and $m=2.0$.

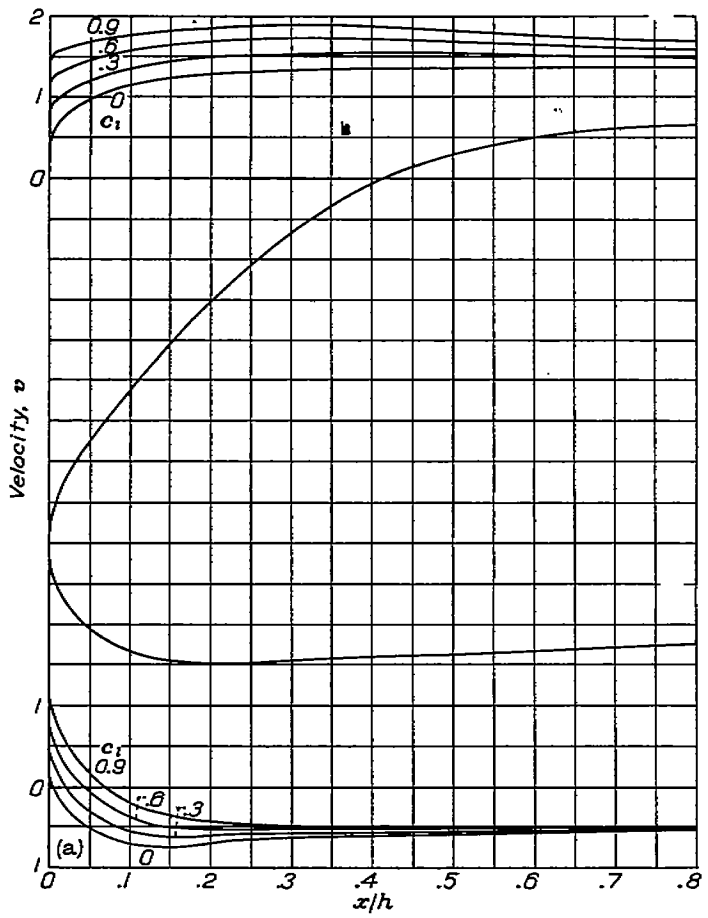

(a) Upper leading edge.

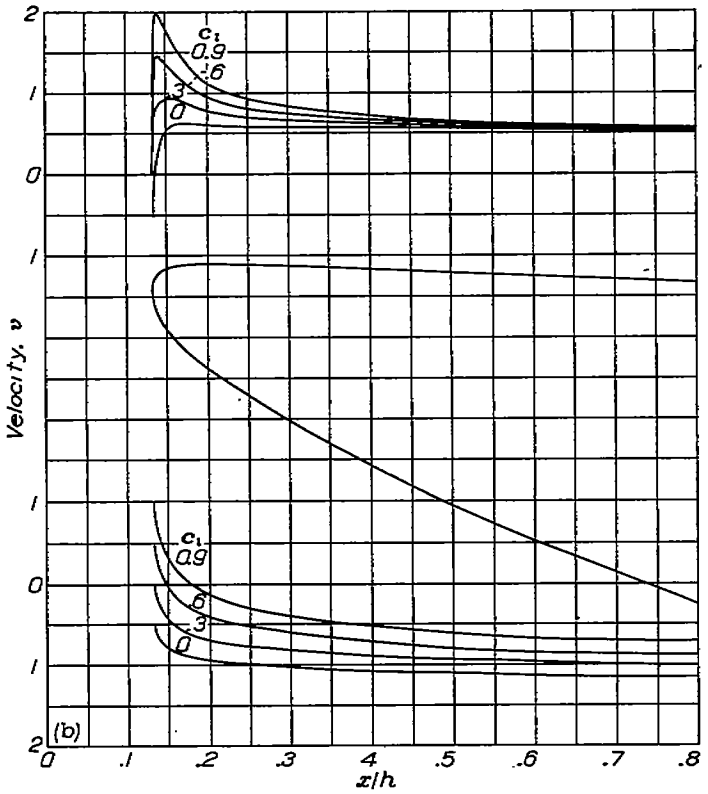

(b) Lower leading edge.

FIGURE 11.—Velocity distribution on upper and lower leading edges of nonsymmetrical duct-inlet section with $s=0.215$ and $m=2.0$. $z_n=0.5$.

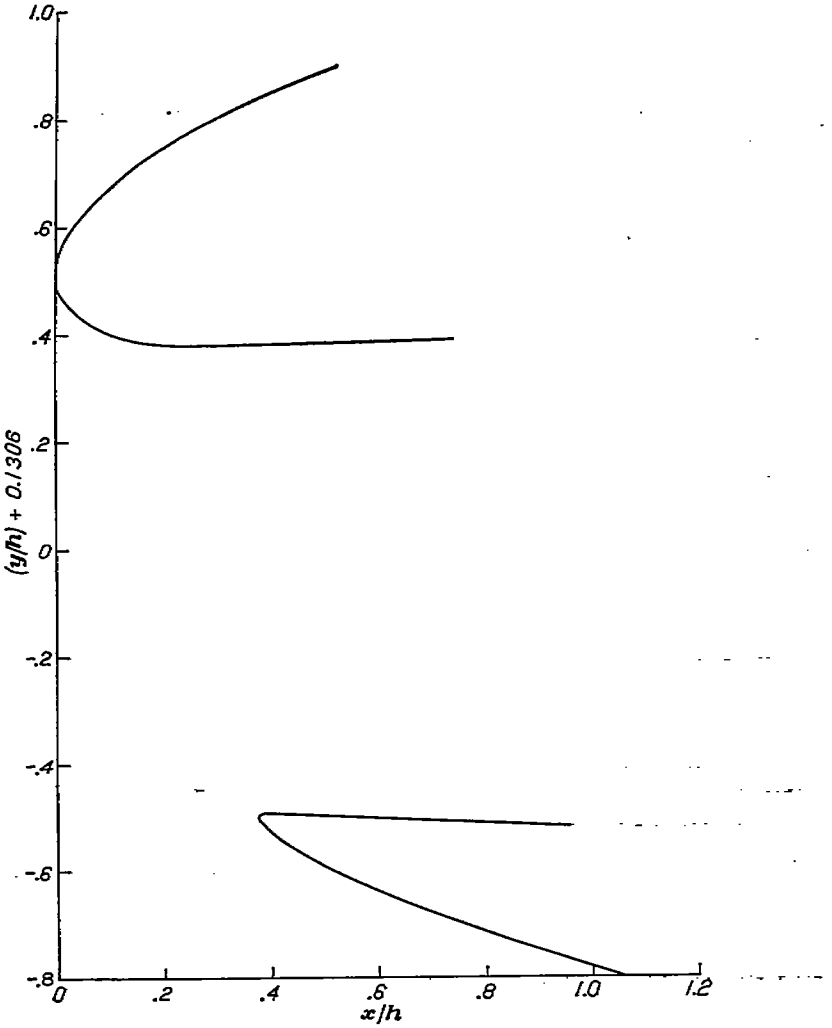

FIGURE 12.—Leading edge of nonsymmetrical duct-inlet section with $s=0.280$ and $m=3.0$. $z_n=1.5$.

CONFORMAL MAPPING OF LEADING-EDGE REGIONS

The requirement that the velocity distribution need be accurately known only near the leading edges permitted the great simplification in the mapping consisting in replacement of the doubly connected region by a simply connected region. The modification of the contour shape far behind the leading edge did not appreciably alter the velocity distribution at the leading edges. Corresponding simplifications can be effected in other problems involving conformal mapping of aerodynamic shapes where only the leading-edge region is of interest.

Thus, for example, the leading-edge region of an isolated airfoil can be regarded as joining a semi-infinite shape, as indicated in figure 13. The mapping of such a contour into a circle is quite simple. The leading-edge contour, z-plane, is mapped onto a semi-infinite chord line, ζ-plane, by the CMF

$$z-\zeta=\Delta x+i\Delta y=(x-\xi)+i(y-\eta) \tag{30}$$

The semi-infinite chord line is mapped onto an infinite straight line, t-plane, by

$$\zeta=t^2 \tag{31}$$

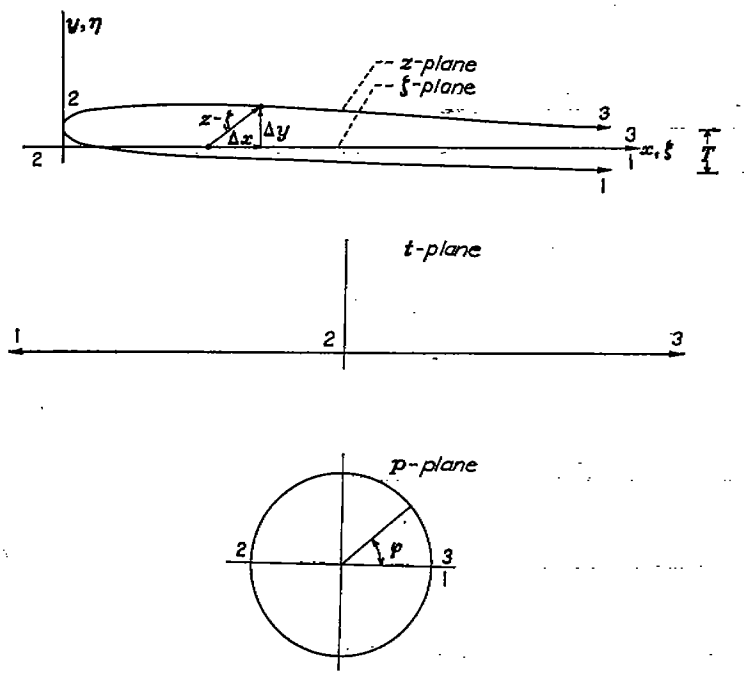

FIGURE 13.—Mapping of leading-edge region for isolated airfoils.

and, in turn, the t-plane contour is mapped onto a unit circle by a bilinear transformation, such as

$$t=i\left(\frac{p+1}{p-1}\right) \tag{32}$$

On the unit circle $p=e^{i\phi}$, equations (30) to (32) give for the coordinates x and y of the leading-edge contour in the physical plane

$$x=\cot^2\frac{\phi}{2}+\Delta x(\phi) \tag{33}$$

$$y=\Delta y(\phi) \tag{34}$$

The mapping of the leading-edge contour by equations (33) and (34) involves little more than the calculation of conjugates.

The velocity distribution is obtained from the complex potential

$$W=\zeta+At \tag{35}$$

in which the term ζ represents the uniform free-stream flow and the term At a circulatory flow around the leading edge. On the leading-edge contour the velocity distribution $|dW/dz|$ becomes

$$v=\frac{\left(1+\frac{A}{2}\tan\frac{\phi}{2}\right)\cot\frac{\phi}{2}\csc^2\frac{\phi}{2}}{\sqrt{\left(\cot\frac{\phi}{2}\csc^2\frac{\phi}{2}-\frac{d\Delta x}{d\phi}\right)^2+\left(\frac{d\Delta y}{d\phi}\right)^2}} \tag{36}$$

A similar development can be made for a cascade of leading-edge regions, which bears the same relation to a cascade of airfoils as the leading-edge region just treated bears to the isolated airfoil.

SAW-TOOTH FUNCTION AS INITIAL APPROXIMATION

In the mapping of semi-infinite contours, it may be required, or it may be simpler, to consider a contour for which the thickness at infinity is finite, as indicated in figure 13. The ordinate function $\Delta y(\phi)$ will in this case be discontinuous at the value of ϕ corresponding to the point at infinity on the physical-plane contour. The calculation of the CMF for such a contour will be simplified if the Cartesian mapping function $\Delta x+i\Delta y$ is considered as the sum of two component Cartesian mapping functions $\Delta_1 x+i\Delta_1 y$ and $\Delta_2 x+i\Delta_2 y$, of which $\Delta_1 x+i\Delta_1 y$ is analytically known and represents a contour with the same thickness at infinity.

Thus, if the thickness at infinity of the contour in the physical plane is T, the "first harmonic" saw-tooth function (fig. 14)

$$\Delta_1 y(\phi)=\frac{T}{\pi}\left(\frac{\pi}{2}-\frac{\phi}{2}\right) \tag{37}$$

will yield a shape with this thickness. The function $\Delta_1 x(\phi)$ conjugate to $\Delta_1 y(\phi)$ may be simply obtained from the integral relation for the conjugate derivative (equation (C3) of reference 5)

$$\frac{d\Delta x(\phi)}{d\phi}=-\frac{1}{4\pi}\int_0^{2\pi}\frac{\Delta y(\phi')-\Delta y(\phi)}{\sin^2\frac{\phi'-\phi}{2}}d\phi' \tag{38}$$

Substitution of equation (37) in equation (38) and integration (using integration by parts) yields

$$\frac{d\Delta_1 x}{d\phi}=\frac{T}{2\pi}\cot\frac{\phi}{2} \tag{39}$$

which by integration gives for $\Delta_1 x$

$$\Delta_1 x=\frac{T}{\pi}\log_e\sin\frac{\phi}{2} \tag{40}$$

The ordinate function derivative is evidently

$$\frac{d\Delta_1 y}{d\phi}=-\frac{T}{2\pi} \tag{41}$$

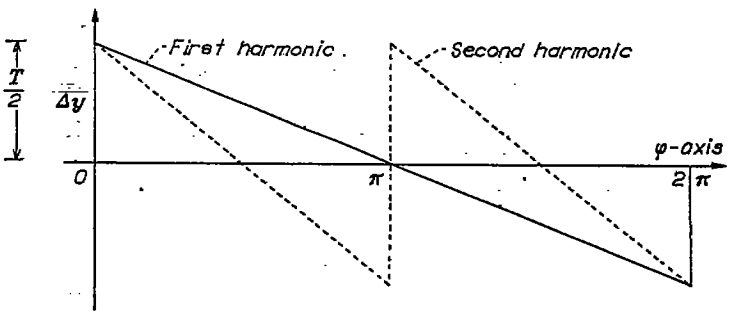

FIGURE 14.—Saw-tooth ordinate functions.

The CMF for a "second harmonic" saw tooth (fig. 14) corresponding to a duct-inlet section with thickness T (of each component contour) at infinity may be obtained from that of the first harmonic saw-tooth function by replacing $\phi/2$ in equations (37), (39), and (40) by ϕ and by doubling the derivatives. Thus, for the second harmonic saw-tooth function

$$\left.\begin{aligned}\Delta_1 y&=\frac{T}{\pi}\left(\frac{\pi}{2}-\phi\right) \quad 0<\phi<\pi\\ \Delta_1 y&=\frac{T}{\pi}\left(\frac{3\pi}{2}-\phi\right) \quad \pi<\phi<2\pi\end{aligned}\right\} \tag{42}$$

$$\frac{d\Delta_1 y}{d\phi}=-\frac{T}{\pi} \tag{43}$$

$$\Delta_1 x=\frac{T}{\pi}\log_e \sin\phi \tag{44}$$

$$\frac{d\Delta_1 x}{d\phi}=\frac{T}{\pi}\cot\phi \tag{45}$$

The duct-inlet shapes corresponding to the second harmonic saw-tooth CMF have been calculated by equations (10) and (11) with $m=1.0$ (no stagger) and for $T=0.1$, 0.2, and 0.3. The contours are shown in figure 15. For these shapes, the velocity infinitely far inside the duct is, by equations (43), (45), and (26) with $\phi=\pi$,

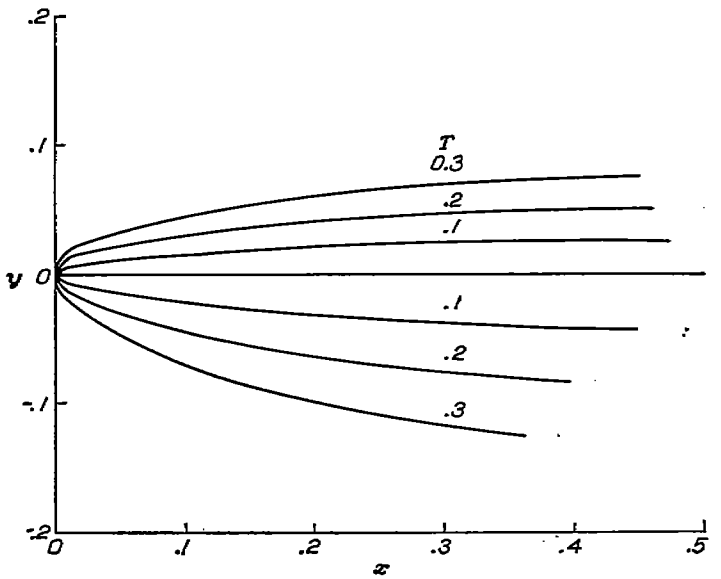

FIGURE 15.—Leading-edge shapes for duct inlet using the second harmonic saw-tooth function. $s=0$; $m=1$.

$$v_{D\infty}=\frac{1-B}{1-T} \tag{46}$$

which, when compared with equation (19), shows the effect of narrowing the duct at infinity.

AIRCRAFT ENGINE RESEARCH LABORATORY,
NATIONAL ADVISORY COMMITTEE FOR AERONAUTICS,
CLEVELAND, OHIO, *April 1, 1947.*

REFERENCES

1. Mutterperl, William: The Conformal Transformation of an Airfoil into a Straight Line and Its Application to the Inverse Problem of Airfoil Theory. NACA ARR No. L4K22a, 1944.
2. Kellogg, Oliver Dimon: Foundations of Potential Theory. Ch. XII, sec. 13, ex. 8, Julius Springer (Berlin), 1929, p. 375.
3. Mutterperl, William: A Solution of the Direct and Inverse Potential Problems for Arbitrary Cascades of Airfoils. NACA ARR No. L4K22b, 1944.
4. von Doenhoff, Albert E., and Horton, Elmer A.: Preliminary Investigation in the NACA Low-Turbulence Tunnel of Low-Drag Airfoil Sections Suitable for Admitting Air at the Leading Edge. NACA ACR, July 1942.
5. Perl, W., and Moses, H. E.: Velocity Distributions on Symmetrical Airfoils in Closed Tunnels by Conformal Mapping. NACA TN No. 1642, 1948.
6. Smith, Norman F.: High-Speed Investigation of Low-Drag Wing Inlets. NACA ACR No. L4I18, 1944.

TABLE I—ORDINATES OF SYMMETRICAL DUCT INLET

[Reference 4, shape 9]

Station (percent chord from leading edge)	Ordinate of outer surface (measured from center line of channel) (percent chord)	Ordinate of inner surface (measured from center line of channel) (percent chord)
0	3.343	3.34
.25	3.660	3.07
.5	3.835	3.05
.75	3.976	3.05
1.25	4.228	3.07
2.5	4.745	3.13
5	5.532	3.25
7.5	6.137	3.36
10	6.652	3.50
15	7.467	3.78
20	8.038	4.08
25	8.593	
30	8.965	4.57
35	9.224	
40	9.379	4.90
45	9.435	
50	9.391	5.10
55	9.240	
60	8.966	4.94
65	8.510	
70	7.804	4.27
75	6.878	
80	5.816	2.54
85	4.679	
90	3.522	1.55
95	2.387	
100	1.314	1.31

TABLE II—ORDINATES AND VELOCITY DISTRIBUTIONS FOR SYMMETRICAL DUCT INLET WITH $s=0$ AND $m=1.0$

[$r=0$; $\phi_H=75.00°$; $\phi_G=285.00°$; $\phi_E=6.882°$; $\phi_C=353.12°$; $h=2.4800$]

ϕ (deg)	x/h	$(y/h)+0.2011$ (ordinate)	Δx	Δy	Velocity, v											
					($v_a=0$; $B=1.00000$)				($v_a=0.5$; $B=-0.38907$)				($v_a=1.0$; $B=-1.55000$)			
					$c_1=0$ $A=0$	0.3 0.58494	0.6 1.16989	0.9 1.75483	0 0	0.3 0.58494	0.6 1.16989	0.9 1.75483	0 0	0.3 0.58494	0.6 1.16989	0.9 1.75483
Upper duct inlet section																
0X7.5	∞	0.2011	*−2.8592	0	1.0000	1.0000	1.0000	1.0000	1.0000	1.0000	1.0000	1.0000	1.0000	1.0000	1.0000	1.0000
1	12.3540	.8662	*−5.1796	1.6534	1.0697	1.1107	1.1517	1.1927	1.0633	1.1043	1.1454	1.1863	1.0580	1.0990	1.1400	1.1810
2	2.8117	1.2098	*−1.2595	2.5076	1.1719	1.2022	1.3524	1.4427	1.1437	1.2340	1.3242	1.4144	1.1201	1.2104	1.3006	1.3909
3	1.0887	.9259	−.5144	1.8018	1.1944	1.3334	1.4724	1.6113	1.1288	1.2678	1.4067	1.5457	1.0739	1.2129	1.3518	1.4908
4	.5162	.7713	−.2265	1.4174	1.2238	1.4157	1.6075	1.7993	1.1018	1.2936	1.4854	1.6773	.9998	1.1916	1.3834	1.5752
5	.2490	.6695	−.1306	1.1644	1.2535	1.5025	1.7514	2.0003	1.0529	1.3018	1.5508	1.7997	.8852	1.1341	1.3830	1.6319
6	.1225	.6121	−.0546	1.0217	1.2460	1.6721	1.9982	2.3243	1.0252	1.3513	1.6774	2.0035	.7571	1.0832	1.4093	1.7354
7	.0524	.5708	−.0115	.9190	1.4799	1.9068	2.3337	2.7606	.9800	1.4069	1.8338	2.2607	.5622	.9891	1.4160	1.8429
8	.0221	.5410	.0400	.8448	1.6354	2.1877	2.7400	3.2923	.8782	1.4305	1.9828	2.5251	.2454	.7977	1.3500	1.9023
9	.0041	.5165	.0699	.7839	1.8827	2.6185	3.3544	4.0902	.7151	1.4509	2.1868	2.9226	.2607	.4751	1.2110	1.9468
10	.0017	.4996	.1060	.7420	2.0239	2.9324	3.8408	4.7493	.3686	1.2770	2.1855	3.0940	1.0150	.1055	.8020	1.7104
11	.0033	.4858	.1307	.7078	1.7745	2.6848	3.5951	4.5053	.1212	.7891	1.6993	2.6096	1.7055	.7952	.1151	1.0263
12	.0136	.4766	.1623	.6849	1.2056	1.9109	2.6161	3.3213	.4691	.2361	.9414	1.6467	1.8687	1.1635	.4583	.2470
13	.0259	.4713	.1879	.6716	.7651	1.2754	1.7857	2.2960	.6167	.1064	.4039	.9142	1.7716	1.2613	.7510	.2407
14	.0471	.4690	.2268	.6659	.4713	.8305	1.1898	1.5490	.6405	.2813	.0780	.4372	1.5697	1.2105	.8512	.4920
15	.0713	.4682	.2655	.6640	.2091	.5609	.8227	1.0845	.6314	.3696	.1078	.1540	1.4090	1.1472	.8854	.6236
16	.1034	.4675	.3168	.6621	.1961	.3947	.5933	.7920	.6210	.4222	.2237	.0250	1.3038	1.1051	.9065	.7079
17	.1385	.4690	.3685	.6659	.1305	.2853	.4401	.5948	.6148	.4601	.3053	.1505	1.2378	1.0830	.9282	.7734
18	.1842	.4705	.4379	.6697	.0858	.2069	.2280	.4491	.6086	.4875	.3664	.2453	1.1889	1.0678	.9467	.8256
19	.2363	.4736	.5131	.6773	.0543	.1480	.2416	.3353	.6008	.5071	.4135	.3198	1.1483	1.0546	.9610	.8673
20	.3067	.4766	.6195	.6849	.0324	.0819	.1740	.2447	.5949	.5240	.4532	.3825	1.1190	1.0482	.9774	.9067
21	.3912	.4789	.7400	.6906	.0172	.0677	.1182	.1687	.5859	.5354	.4849	.4344	1.0900	1.0395	.9890	.9385
22	.5227	.4843	.9389	.7040	.0069	.0374	.0679	.0984	.5435	.5130	.4825	.4519	1.0034	.9729	.9424	.9119
23	.7401	.4950	*1.2595	.7306	.0017	.0167	.0318	.0468	.5432	.5281	.5131	.4980	.9985	.9835	.9684	.9534
24	∞	.2011	*3.0449	0	0	0	0	0	1.3891	1.3891	1.3891	1.3891				
Lower duct-inlet section																
24	∞	−0.2011	*3.0449	0	0	0	0	0	1.3891	1.3891	1.3891	1.3891	2.5500	2.5500	2.5500	2.5500
25	0.7401	−.4950	*1.2595	−.7306	.0017	.0134	.0284	.0434	.5432	.5582	.5732	.5883	.9985	1.0135	1.0286	1.0436
26	.5227	−.4843	.9389	−.7040	.0069	.0237	.0542	.0847	.5435	.5740	.6045	.6350	1.0034	1.0340	1.0645	1.0950
27	.3912	−.4789	.7400	−.6906	.0172	.0323	.0839	.1344	.5859	.6365	.6870	.7375	1.0900	1.1407	1.1910	1.2416
28	.3067	−.4766	.6195	−.6849	.0324	.0384	.1091	.1799	.5949	.6656	.7363	.8071	1.1190	1.1897	1.2605	1.3313
29	.2363	−.4736	.5131	−.6773	.0543	.0393	.1329	.2266	.6008	.6944	.7888	.8817	1.1483	1.2419	1.3356	1.4292
30	.1842	−.4705	.4379	−.6697	.0858	.0364	.1655	.2776	.6086	.7297	.8508	.9719	1.1889	1.3100	1.4311	1.5523
31	.1385	−.4690	.3685	−.6659	.1305	.0243	.1791	.3339	.6148	.7696	.9244	1.0792	1.2378	1.3926	1.5473	1.7021
32	.1034	−.4675	.3168	−.6621	.1961	.0026	.2012	.3999	.6210	.8196	1.0182	1.2169	1.3038	1.5024	1.7010	1.8997
33	.0713	−.4682	.2655	−.6640	.2991	.0375	.2246	.4864	.6314	.8932	1.1550	1.4168	1.4090	1.6708	1.9326	2.1944
34	.0471	−.4690	.2268	−.6659	.4713	.1120	.2472	.6065	.6405	.9998	1.3590	1.7183	1.5697	1.9289	2.2882	2.6474
35	.0259	−.4713	.1879	−.6716	.7651	.2548	.2555	.7659	.6197	1.1271	1.6374	2.1477	1.7717	2.2819	2.7923	3.3026
36	.0136	−.4766	.1623	−.6849	1.2056	.5004	.2048	.9100	.4691	1.1743	1.8795	2.5848	1.8687	2.5789	3.2792	3.9844
37	.0033	−.4858	.1307	−.7078	1.7745	.8642	.0461	.9563	.1212	1.0314	1.9417	2.8520	1.7055	2.6157	3.5261	4.4364
38	.0017	−.4996	.1060	−.7420	2.0239	1.1155	.2070	.7014	.3686	.5399	1.4484	2.3568	1.0150	1.9234	2.8319	3.7403
39	.0041	−.5165	.0699	−.7839	1.8827	1.1468	.4109	.3249	.7151	.0208	.7867	1.4925	.2607	.9966	1.7325	2.4683
40	.0221	−.5410	.0400	−.8448	1.6354	1.0881	.5308	.0214	.8782	.3259	.2264	.7786	.2454	.3069	.8592	1.4114
41	.0524	−.5708	−.0115	−.9190	1.4799	1.0531	.6261	.1992	.9800	.5531	.1262	.3007	.5622	.1353	.2916	.7185
42	.1225	−.6121	−.0546	−1.0217	1.2460	1.0198	.6937	.3676	1.0252	.8091	.3730	.0468	.7571	.4310	.1049	.2213
43	.2490	−.6695	−.1306	−1.1644	1.2535	1.0046	.7557	.5068	1.0529	.8040	.5551	.3062	.8852	.6363	.3874	.1385
44	.5162	−.7713	−.2265	−1.4174	1.2238	1.0320	.8402	.6484	1.1018	.9100	.7182	.5264	.9998	.8080	.6162	.4243
45	1.0887	−.9259	−.5144	−1.8018	1.1944	1.0554	.9165	.7775	1.1288	.9828	.8509	.7119	1.0739	.9249	.7960	.6570
46	2.8117	−1.2098	−1.2595	−2.5076	1.1719	1.0317	.9914	.9012	1.1437	1.0535	.9632	.8730	1.1201	1.0299	.9396	.8494
47	12.3540	−.8662	*−5.1796	−1.6534	1.0697	1.0287	.9877	.9467	1.0633	1.0228	.9813	.9403	1.0580	1.0170	.9760	.9350

* Obtained by graphical integration.

TABLE III—ORDINATES AND VELOCITY DISTRIBUTIONS FOR NONSYMMETRICAL DUCT INLET WITH $s=0.132$ AND $m=1.5$

[$\tau=-0.0341$; $\phi_H=109°$; $\phi_G=289.31°$; $\phi_E=6.51°$; $\phi_C=353.12°$; $h=2.6667$]

ϕ (deg)	x/h	$(y/h)+0.1650$ (ordinate)	Velocity, v ($v_s=0.5$; $B=-0.38907$)			
			$c_l=0$ $A=0.01518$	0.3 0.38901	0.6 0.76285	0.9 1.13668
Upper duct-inlet section						
0 x 7.5	∞	0.1650	1.0000	1.0000	1.0000	1.0000
1	6.3026	.7850	1.0751	1.1162	1.1571	1.1985
2	1.2949	1.1053	1.2487	1.3510	1.4533	1.5556
3	.4257	.8407	1.2072	1.3709	1.5346	1.6983
4	.1693	.6965	1.1023	1.3316	1.5608	1.7900
5	.0559	.6016	.9625	1.2689	1.5753	1.8817
6	.0159	.5481	.7539	1.1475	1.5712	1.9349
7	0	.5096	.4219	.8743	1.3267	1.7790
8	.0057	.4818	.0418	.4934	.9451	1.3968
9	.0134	.4590	.2796	.1409	.5614	.9820
10	.0296	.4433	.5018	.1377	.2264	.5905
11	.0455	.4304	.6440	.3338	.0236	.2866
12	.0667	.4219	.7169	.4593	.2018	.0558
13	.0876	.4169	.7479	.5357	.3235	.1112
14	.1153	.4147	.7295	.5609	.3022	.2235
15	.1446	.4140	.6994	.5654	.4315	.2975
16	.1804	.4133	.6740	.5663	.4586	.3509
17	.2184	.4147	.6561	.5687	.4813	.3939
18	.2655	.4161	.6406	.5700	.4995	.4290
19	.3182	.4190	.6252	.5693	.5134	.4576
20	.3875	.4219	.6128	.5697	.5267	.4837
21	.4697	.4240	.5985	.5673	.5361	.5049
22	.5653	.4290	.5515	.5324	.5133	.4942
23	.8010	.4390	.5469	.5374	.5279	.5183
24	∞	.1650	1.3891	1.3891	1.3891	1.3891
Lower duct-inlet section						
24	∞	−0.2100	1.3891	1.3891	1.3891	1.3891
25	0.8062	−.4840	.5308	.5495	.5592	.5689
26	.6058	−.4740	.5373	.5571	.5760	.5967
27	.4855	−.4690	.5775	.6105	.6430	.6766
28	.4088	−.4669	.5843	.6309	.6775	.7241
29	.3452	−.4640	.5887	.6507	.7127	.7748
30	.2985	−.4611	.5954	.6760	.7567	.8374
31	.2576	−.4597	.6010	.7046	.8081	.9116
32	.2264	−.4583	.6073	.7406	.8740	1.0073
33	.1978	−.4590	.6198	.7954	.9714	1.1474
34	.1764	−.4597	.6322	.8733	1.1143	1.3554
35	.1574	−.4619	.6157	.9536	1.2915	1.6294
36	.1462	−.4669	.4874	.9380	1.3887	1.8394
37	.1362	−.4754	.2085	.7658	1.3231	1.8804
38	.1324	−.4883	.1844	.3848	.9540	1.5232
39	.1325	−.5040	.5214	.0187	.4840	.9866
40	.1435	−.5268	.7311	.3237	.0837	.4911
41	.1614	−.5546	.8833	.5481	.2128	.1224
42	.2081	−.5931	.9699	.7018	.4336	.1055
43	.2903	−.6466	1.0262	.8159	.6036	.3913
44	.4663	−.7415	1.1043	.9347	.7651	.5955
45	.8267	−.8857	1.1660	1.0375	.9091	.7806
46	1.8893	−1.1503	1.2070	1.1202	1.0334	.9466
47	7.6068	−.8300	1.0715	1.0330	.9945	.9560

TABLE IV—ORDINATES AND VELOCITY DISTRIBUTIONS FOR NONSYMMETRICAL DUCT INLET WITH $s=0.215$ AND $m=2.0$

[$\tau=-0.0374$; $\phi_H=114.98°$; $\phi_G=289.12°$; $\phi_E=6.19°$; $\phi_C=353.12°$; $h=2.8525$]

ϕ (deg)	x/h	$(y/h)+0.1206$ (ordinate)	Velocity, v ($v_s=0.5$; $B=-0.38907$)			
			$c_l=0$ $A=0.03038$	0.3 0.30445	0.6 0.57852	0.9 0.85259
Upper duct-inlet section						
0 x 7.5	∞	0.1206	1.0000	1.0000	1.0000	1.0000
1	3.6137	.7002	1.0655	1.1068	1.1481	1.1895
2	.6084	.9997	1.3818	1.5022	1.6226	1.7430
3	.1545	.7522	1.2524	1.4466	1.6408	1.8350
4	.0444	.6175	1.2326	1.1822	1.4317	1.6813
5	.0019	.5288	.6065	.9191	1.2316	1.5442
6	.0009	.4788	.1917	.5156	.8396	1.1636
7	.0091	.4427	.1527	.1446	.4419	.7393
8	.0302	.4167	.3887	.1260	.1366	.3993
9	.0489	.3954	.5511	.3185	.0860	.1466
10	.0727	.3807	.6559	.4525	.2491	.0458
11	.0943	.3687	.7284	.5498	.3711	.1925
12	.1194	.3607	.7656	.6112	.4567	.3023
13	.1425	.3560	.7797	.6474	.5151	.3827
14	.1781	.3540	.7553	.6461	.5370	.4278
15	.2037	.3534	.7217	.6324	.5430	.4537
16	.2399	.3527	.6929	.6194	.5461	.4726
17	.2778	.3540	.6717	.6111	.5506	.4900
18	.3240	.3554	.6531	.6036	.5541	.5046
19	.3751	.3580	.6350	.5954	.5558	.5162
20	.4417	.3607	.6203	.5895	.5587	.5279
21	.5200	.3627	.6039	.5814	.5588	.5363
22	.6390	.3674	.5550	.5412	.5273	.5134
23	.8325	.3767	.5485	.5416	.5347	.5277
24	∞	.1206	1.3891	1.3891	1.3891	1.3891
Lower duct-inlet section						
24	∞	−0.2300	1.3891	1.3891	1.3891	1.3891
25	0.8390	−.4801	.5384	.5455	.5526	.5598
26	.6587	−.4768	.5345	.5491	.5638	.5784
27	.5423	−.4721	.5738	.5983	.6228	.6474
28	.4716	−.4701	.5798	.6145	.6492	.6839
29	.4130	−.4675	.5836	.6299	.6763	.7226
30	.3702	−.4648	.5900	.6504	.7108	.7713
31	.3328	−.4635	.5957	.6736	.7512	.8289
32	.3043	−.4621	.6028	.7030	.8033	.9036
33	.2782	−.4628	.6165	.7490	.8815	1.0140
34	.2587	−.4635	.6328	.8140	.9953	1.1765
35	.2414	−.4655	.6221	.8744	1.1266	1.3789
36	.2311	−.4701	.5057	.8361	1.1665	1.4970
37	.2215	−.4781	.2602	.6000	1.0597	1.4595
38	.2182	−.4901	.0828	.3270	.7367	1.1464
39	.2160	−.5048	.3965	.0215	.3535	.7385
40	.2234	−.5261	.6176	.3004	.0168	.3339
41	.2355	−.5522	.7928	.5207	.2486	.0235
42	.2702	−.5882	.9072	.6814	.4557	.2299
43	.3306	−.6382	.9900	.8060	.6215	.4309
44	.4609	−.7269	1.0874	.9356	.7838	.6320
45	.7152	−.8617	1.1876	1.0673	.9471	.8269
46	1.4561	−1.1091	1.2634	1.1787	1.0939	1.0091
47	5.3157	−.8096	1.0653	1.0289	.9924	.9559

TABLE V—ORDINATES OF NONSYMMETRICAL DUCT INLET WITH $s=0.280$ AND $m=3.0$

[$n=1.5$; $\tau=0.0310$; $h=2.6813$]

θ (deg)	φ (deg)	x/h	$(y/h)+0.1306$ (ordinate)
Upper duct inlet section			
0 x 7.5	0	∞	0.1306
1	5.004	6.4980	.7519
2	10.032	1.1177	1.0729
3	15.108	.3013	.8077
4	20.256	.0902	.6632
5	25.503	.0130	.5682
6	30.874	.0011	.5145
7	36.398	.0074	.4759
8	42.103	.0312	.4481
9	48.021	.0539	.4252
10	54.184	.0829	.4004
11	60.625	.1007	.3966
12	67.380	.1407	.3880
13	74.488	.1704	.3830
14	81.969	.2059	.3809
15	89.870	.2425	.3801
16	98.213	.2851	.3794
17	107.018	.3298	.3809
18	116.298	.4063	.3823
19	126.031	.4410	.3851
20	136.207	.5159	.3880
21	146.773	.6037	.3901
22	157.658	.7349	.3952
23	168.770	.9460	.4052
24	180.000	∞	.1306
Lower duct inlet section			
24	180.000	∞	−0.2451
25	191.230	0.9017	−.5197
26	202.342	.7664	−.5097
27	213.227	.6518	−.5046
28	223.793	.5799	−.5025
29	233.909	.5222	−.4996
30	243.707	.4817	−.4968
31	253.982	.4473	−.4954
32	261.787	.4232	−.4939
33	270.130	.4024	−.4946
34	278.031	.3895	−.4954
35	285.517	.3802	−.4975
36	292.620	.3799	−.5025
37	299.375	.3825	−.5111
38	305.816	.3946	−.5239
39	311.979	.4119	−.5397
40	317.897	.4454	−.5626
41	323.602	.4926	−.5904
42	329.126	.5787	−.6290
43	334.497	.7176	−.6827
44	339.744	.9830	−.7777
45	344.892	1.5028	−.9222
46	349.908	2.9347	−1.1874
47	354.996	10.1469	−.8604